

## Crest instabilities of gravity waves. Part 3. Nonlinear development and breaking

By MICHAEL S. LONGUET-HIGGINS<sup>1</sup>  
AND DOUGLAS G. DOMMERMUTH<sup>2</sup>

<sup>1</sup>Institute for Nonlinear Science, University of California, San Diego, La Jolla,  
CA 92093-0402, USA

<sup>2</sup>Naval Hydrodynamics Division, Science Applications International Corporation,  
10260 Campus Point Drive, San Diego, CA 92121, USA

(Received 15 December 1995 and in revised form 14 August 1996)

The ‘almost-highest wave’, which is the asymptotic form of the flow in a steep irrotational water wave of less than the limiting height, was recently shown to be unstable to infinitesimal disturbances (see Longuet-Higgins & Cleaver 1994). It was also shown numerically that the lowest eigenfrequency is asymptotic to that of the lower superharmonic instability of a progressive wave in deep water (Longuet-Higgins, Cleaver & Fox 1994). In the present paper these calculations are revised, indicating the presence of more than one such instability, in agreement with recent calculations on steep periodic and solitary waves (Longuet-Higgins & Tanaka 1997).

The nonlinear development of the fastest-growing instability is also traced by a boundary-integral time-stepping method and the initial, linear growth rate is confirmed. The subsequent, nonlinear stages of growth depend as expected on the sign of the initial perturbation. Perturbations of one sign lead to the familiar overturning of the wave crest. Perturbations of the opposite sign lead to a smooth transition of the wave to a lower progressive wave having nearly the same total energy, followed by a return to a wave of almost the initial wave height. This appears to be the beginning of a nonlinear recurrence phenomenon.

---

### 1. Introduction

In a recent paper (Longuet-Higgins & Cleaver 1994) it was shown that the local flow near the crest of a steep, progressive gravity wave on water is itself subject to an exponentially growing instability. To distinguish it from instabilities involving the whole wave, this was called a ‘crest instability’. In a second paper (Longuet-Higgins, Cleaver & Fox 1994) it was further shown numerically that the crest instability is the asymptotic form of the lowest superharmonic instability of a complete, periodic gravity wave in deep water when the wave steepness  $ak$  tends to its limiting value  $(ak)_{max} = 0.4423$ . As shown by Tanaka (1983) this instability first occurs when  $ak = 0.4292$ , the value at which the total energy  $E$  attains its first maximum (see also Saffman 1985). For solitary waves, a parallel result was demonstrated numerically by Tanaka (1986).

In the above work all of the calculations, whether analytic or purely numerical, were carried out on the basis of linear perturbation theory, and the departures from a steady, nonlinear wave were assumed infinitesimally small. An interesting paper by Tanaka *et al.* (1987) traced the subsequent nonlinear development of the fastest-growing instability for the solitary wave by numerical time stepping. Depending on the

sign of the initial perturbation, it either developed into a plunging breaker or else underwent a smooth transition to a solitary wave of lower amplitude and nearly the same total energy. A similar investigation for periodic waves in deep water was attempted by Jillians (1988) with partial success (see below). Meanwhile the general interest in the subject has intensified owing to its relevance to wave breaking and turbulent mixing in the uppermost layer of the ocean, and to the microstructure of the sea surface.

The purpose of the present paper is twofold. First we revise and extend the linear stability calculations on deep-water waves reported in Longuet-Higgins & Cleaver (1994) and Longuet-Higgins *et al.* (1994). The need for such revision was prompted by a recent independent investigation by Tanaka (1995), undertaken at the request of one of us (M.S.L.-H.).† Our results are described in §3 below.

Our second and main purpose in this paper is to follow by numerical time stepping the nonlinear development of the fastest-growing crest instability of a periodic wave. The approach adopted is slightly different from that of Tanaka *et al.* (1987) or Jillians (1988). Those authors used as initial values for the time stepping a numerically determined normal-mode instability for the complete wave. Here we use instead the lowest crest instability, as calculated in the present paper.

The nonlinear calculation is described in general terms in §4, and the results are given in §5. As expected, the nonlinear development of the instability depends crucially on the sign of the initial (linear) perturbation. A perturbation of positive sign leads on to overturning of the wave crest in the familiar manner (see figure 9). One might have expected a perturbation of negative sign to lead initially to a wave crest with a slight concavity on the forward face but this is not the case. Instead the wave undergoes a smooth transition to a periodic wave of lower amplitude and then returns to a wave of almost the same amplitude, in a kind of recurrence phenomenon. Thus the behaviour is similar to that of the crest instability of a solitary wave, except that for a solitary wave the period of recurrence is infinite.

## 2. Initial conditions: linear perturbation theory

In the theory of the almost-highest wave (Longuet-Higgins & Fox 1977, 1978) the flow near the crest of a steep, irrotational gravity wave is characterized by the horizontal particle velocity  $q$  at the crest of the wave, as seen in a reference frame moving horizontally with the phase speed. Together with gravity  $g$  this defines a characteristic length scale

$$l = q^2/2g \quad (2.1)$$

and a small parameter

$$\epsilon^2 = q^2/2c_0^2 \quad (2.2)$$

where  $c_0$  is the linear phase speed given by

$$c_0^2 = g/k = gL/2\pi, \quad (2.3)$$

$k$  and  $L$  being the wavenumber and wavelength.

The limiting form of the wave crest as  $\epsilon \rightarrow 0$  was determined by Longuet-Higgins & Fox (1977) and is shown in figure 7 of that paper. If axes of  $x$  and  $y$  are chosen as horizontal (opposite to the direction of propagation) and vertically upwards, then we can define

$$z = y - ix, \quad \chi = \phi + i\psi, \quad (2.4)$$

† The details of Tanaka's calculations and an analysis of the results are given in the paper by Longuet-Higgins & Tanaka (1997).

where  $\phi$  and  $\psi$  are the velocity potential and streamfunction. For large values of  $z$  we have

$$z \sim \left(\frac{3}{2}i\chi\right)^{2/3} \quad \text{as } |\chi| \rightarrow \infty, \quad \psi \leq 0, \quad (2.5)$$

corresponding to Stokes's 120° corner flow. Generally, the unperturbed flow is expressed as a series

$$z = (\delta + i\chi)^{2/3} B(\omega), \quad B = \sum_{n=0}^{\infty} B_n \omega^n, \quad (2.6)$$

where

$$\omega = \frac{\delta - i\chi}{\delta + i\chi} \quad (2.7)$$

and  $\delta$  is a constant at our disposal ( $\delta$  was taken to be  $10^{3/2}$ ). The series (2.6) is assumed to converge inside and on the circle  $|\omega| = 1$  which corresponds to the unperturbed free surface. By applying suitable conditions on the boundary, the coefficients  $B_0, B_1, \dots, B_{90}$  were determined to a high degree of accuracy.

The normal-mode perturbations of this flow were calculated in Longuet-Higgins & Cleaver (1994). We write

$$z = Z + \zeta, \quad (2.8)$$

where  $Z$  is the previously determined flow, given by equation (2.6) and  $\zeta$  is a small perturbation. The free surface is defined by  $\psi = F(\phi, t)$  and only terms linear in  $\zeta$  and  $F$  are retained. The kinematic and dynamical boundary conditions combined then lead to a single (complex) condition to be satisfied on  $\psi = 0$ . The perturbations  $\zeta$  and  $F$  are expanded in series:

$$\left. \begin{aligned} \zeta &= \sum_{n=0}^{\infty} (b_n + ia_n) \omega^n, \\ F &= \sum_{n=1}^{\infty} (c_n \cos n\tau + d_n \sin n\tau), \end{aligned} \right\} \quad (2.9)$$

where  $e^{i\tau} = \omega$  and the coefficients  $a_n, b_n, c_n, d_n$  depend on the time  $t$  only. Assuming a time dependence  $e^{\beta t}$  and equating coefficients of  $\cos n\tau$  and  $\sin n\tau$  in the boundary conditions as far as  $n = N$ , say, one is led to a set of  $(4N+2)$  simultaneous linear equations for the vector

$$\mathbf{x} = (a_0, a_1, \dots, a_N; b_0, b_1, \dots, b_N; c_1, \dots, c_N; d_1, \dots, d_N) \quad (2.10)$$

in the form

$$\beta \mathbf{A} \mathbf{x} = \mathbf{B} \mathbf{x} \quad (2.11)$$

where  $\mathbf{A}$  and  $\mathbf{B}$  are matrices of order  $(4N+2)$ . The numerical solution of these equations, for a sufficiently large value of the truncation parameter  $N$ , then yields the required set of eigenvectors  $\beta$  and the corresponding eigenvector  $\mathbf{x}$ , which in turn yields a normal-mode perturbation. There is always one mode in which  $\beta = 0$ ,  $a_0 \neq 0$  and all the other coefficients  $a_n$  vanish. This solution corresponds to a perturbation consisting of a pure phase shift. In Longuet-Higgins *et al.* (1994), the results of Longuet-Higgins & Cleaver (1994) for vanishingly small  $\epsilon$  were extended to positive values of  $\epsilon$  by matching the 'inner' solution for the flow near the crest (that is to say when  $z = O(\epsilon^2)$ ), to an 'outer' flow representing the rest of the wave. The matching process requires a modification to the inner flow by an amount of order  $\epsilon^{3(\lambda-1)}$ , where  $\lambda$  is the lowest positive root of

$$\frac{\pi\lambda}{2} \tan \frac{\pi\lambda}{2} = -\frac{\pi}{2\sqrt{3}}, \quad (2.12)$$

hence  $\lambda = 1.8027$ . Once the modification is made, the calculation of the normal-mode perturbations to this flow can be carried out as before.

### 3. Results of the linear perturbation analysis

In Longuet-Higgins & Cleaver (1994), equations (2.5) were solved numerically for  $N \leq 50$ , using a standard FORTRAN subroutine SGEEV which unfortunately developed significant errors, when  $N$  exceeded about 20. These were only later detected. We have now used a more robust routine which simply determines the sign of the determinant

$$D(\beta) \equiv \|\beta\mathbf{A} - \mathbf{B}\|. \quad (3.1)$$

Hence the zeros of  $D(\beta)$  could be found by a straightforward bracketing technique. The largest positive eigenvalue  $\beta_1$  determined by this method is shown in table 1 for  $N = 60(2)80$  in the column under  $\epsilon = 0$ . It appears to be converging to a value near

$$\beta_1 = 0.0434. \quad (3.2)$$

This differs significantly from the value 0.0544 in table 1 of Longuet-Higgins & Cleaver, but is close to the value (0.0435) found by Cleaver in his PhD dissertation (Cleaver 1981), obtained by the use of a Shanks transform.

The remaining columns of table 1 show the corresponding values of  $\beta_1$  when  $\epsilon = 0.02(0.02)0.14$ . When  $\epsilon > 0.15$  convergence is difficult to obtain. All the values of  $\beta_1$  at  $N = 80$  are plotted against  $\epsilon$  in figure 1. It will be seen that  $\beta_1$  decreases monotonically with  $\epsilon$ .

From equation (2.9) we should expect small departures of  $\beta_1$  from its value at  $\epsilon = 0$  to vary as  $\epsilon^{3(\lambda-1)}$ . In figure 1 we show the curve

$$\beta_1 = 0.0434 - C\epsilon^{3(\lambda-1)}, \quad (3.3)$$

where  $C = 0.046$  is an empirically determined constant.

The calculations also suggested the presence of a second positive zero of  $D(\beta)$  at around 0.01; see table 2. This implies a second exponentially growing mode, as was found also by Tanaka (1995).

For periodic waves on deep water, the parameter  $\epsilon$  is related to the wave steepness  $ak$  by the formula

$$ak = 0.4432 - 0.5\epsilon^2 - 0.160\epsilon^3 \cos(2.143 \ln \epsilon - 1.54) \quad (3.4)$$

(see Longuet-Higgins & Fox 1978, equation (5.4)), so that we may plot the scaled growth rate ( $\beta_n/\epsilon$ ) against  $ak$ . Thus figure 2 shows  $\beta_n/\epsilon$  plotted against  $ak$  and compared with the growth rates  $\lambda_n$  as calculated by Tanaka (1995) for steep periodic waves of less than the limiting steepness. Although Tanaka's calculations were not carried beyond about  $ak = 0.4424$  it is clear that the values of  $\lambda$  or  $\beta_1$  derived from the theory of the almost-highest wave do indeed form a satisfactory asymptote to Tanaka's values. Figures 1 and 2 should be regarded as superseding figures 4 and 5 of Longuet-Higgins *et al.* (1994).

A more stringent comparison is made in figure 3, which shows the squared eigenvalues  $\beta_n^2$  compared to Tanaka's scaled eigenvalues, as a function of  $\epsilon = q/\sqrt{2c_0}$ . In particular the limiting value  $\beta_1^2 = 0.00188$  is a good match to Tanaka's calculations.

After determining the eigenfrequencies  $\beta_n$ , the calculation of the eigenfunctions was carried out by setting  $a_0$  or  $a_1$  equal to 1 and then solving all but one of equations (2.9)

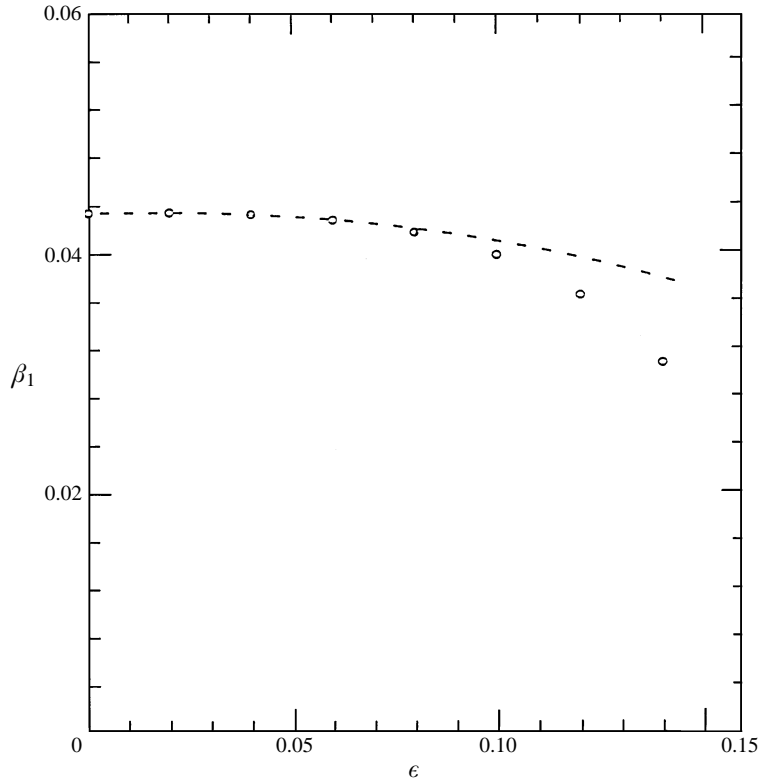


FIGURE 1. The positive growth rate  $\beta_1$  of the lowest crest instability, plotted against  $\epsilon$ . The broken curve represents the asymptotic formula (3.3).

$N \setminus \epsilon$	0.00	0.02	0.04	0.06	0.08	0.10	0.12	0.14
60	0.04325	0.04320	0.04299	0.04251	0.04167	0.04020	0.03749	0.03224
62	0.04327	0.04323	0.04301	0.04254	0.04168	0.04016	0.03737	0.03199
64	0.04330	0.04325	0.04304	0.04256	0.04169	0.04012	0.03725	0.03175
66	0.04332	0.04328	0.04306	0.04258	0.04169	0.04008	0.03714	0.03153
68	0.04334	0.04330	0.04308	0.04260	0.04169	0.04004	0.03702	0.03134
70	0.04336	0.04331	0.04310	0.04261	0.04169	0.04000	0.03691	0.03116
72	0.04337	0.04333	0.04311	0.04262	0.04168	0.03996	0.03681	0.03101
74	0.04339	0.04334	0.04313	0.04263	0.04168	0.03991	0.03671	0.03089
76	0.04340	0.04335	0.04314	0.04264	0.04167	0.03987	0.03661	0.03081
78	0.04340	0.04336	0.04314	0.04264	0.04165	0.03982	0.03652	0.03078
80	0.04340	0.04336	0.04315	0.04264	0.04164	0.03978	0.03645	0.03079

TABLE 1. Calculated values of the growth rate  $\beta_1$

for the remaining coefficients. This yields  $\zeta(\phi, \psi)$  and  $F(\phi)$  by equations (2.7). However, since the free surface is given by  $\psi = F$ , not  $\psi = 0$ , we have for the surface profile to calculate

$$y = Y(\phi, 0) + \left[ F(\phi) \frac{\partial Y}{\partial \psi}(\phi, 0) + \eta(\phi, 0) \right] e^{\beta t}. \quad (3.5)$$

We write this as

$$y = Y + \alpha \Delta y e^{\beta t}, \quad (3.6)$$

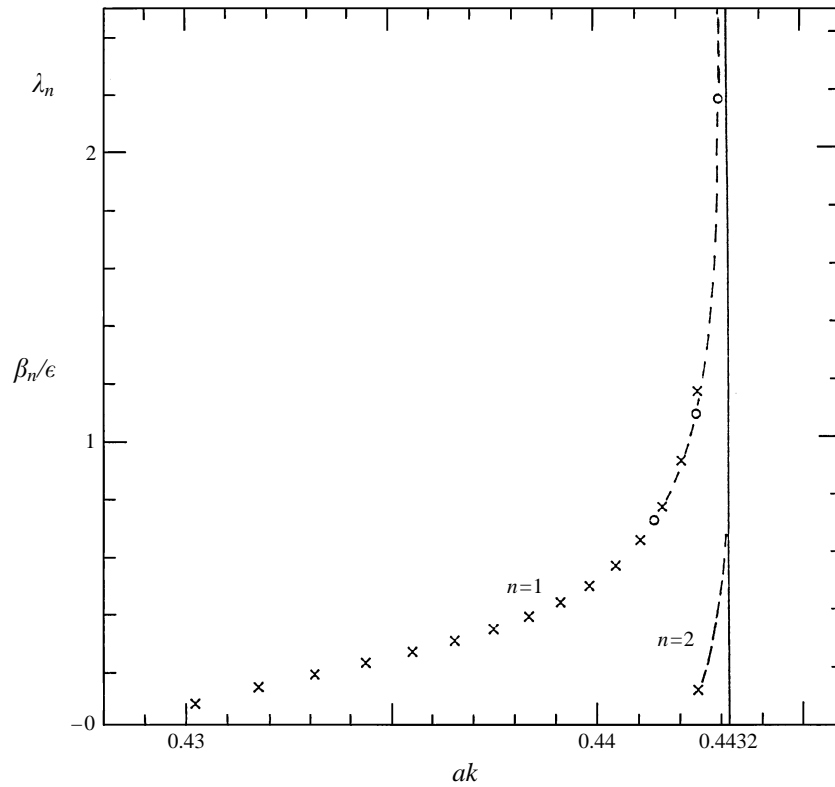


FIGURE 2. Growth rates  $\lambda_n$  of the two lowest superharmonic instabilities of steep periodic waves, as calculated by Tanaka (1995) (crosses). The circles are values of  $\beta_n/\epsilon$  from figure 1 of this paper.

$N \setminus \epsilon$	0.00	0.02	0.04	0.06
60	0.00731	0.00758	0.00838	0.00873
62	0.00763	0.00787	0.00858	0.00878
64	0.00790	0.00812	0.00875	0.00881
66	0.00814	0.00834	0.00889	0.00883
68	0.00835	0.00853	0.00902	0.00884
70	0.00853	0.00869	0.00912	0.00883
72	0.00869	0.00884	0.00921	0.00882
74	0.00883	0.00897	0.00929	0.00880
76	0.00895	0.00908	0.00935	0.00878
78	0.00906	0.00917	0.00941	0.00874
80	0.00915	0.00926	0.00945	0.00870

TABLE 2. Calculated values of  $\beta_2$

where  $\Delta y$  denotes the expression in square brackets on the right of (3.5), normalized so that

$$\max |\Delta y| = 1. \quad (3.7)$$

Essentially  $\Delta y$  gives the form of the perturbation. In figure 4,  $\Delta y$  is plotted against the unperturbed coordinate  $x/l$  with  $\phi$  as parameter. The curves are shown for  $\epsilon = 0$  and 0.08. Each curve has a relatively sharp maximum when  $x < 0$  (on the forward face of

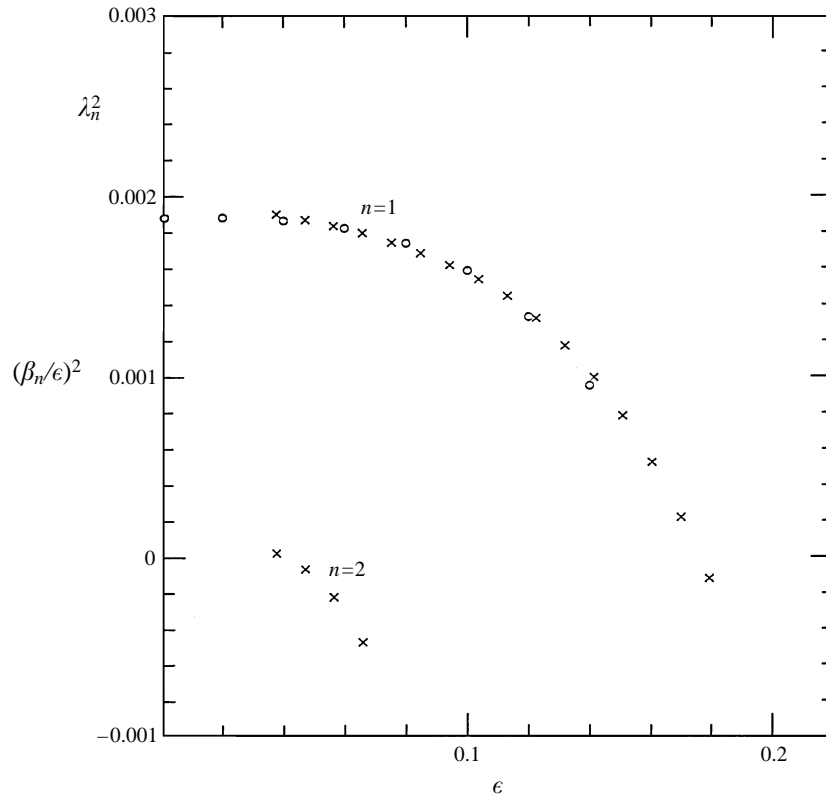


FIGURE 3. Graph of  $\beta_n^2$  (circles, this paper) and  $(\epsilon\lambda_n)^2$  (crosses, Tanaka 1995) against  $\epsilon$ .

the wave) and a less pronounced minimum on the rear face. There is little difference between the curves, however.

Figure 5 shows a comparison of the eigenfunction corresponding to  $\epsilon = 0.08$  with Tanaka's calculated eigenfunction when  $\omega = 0.92$  ( $\epsilon = q/\sqrt{2c_0} = 0.07533$ ). The curves are similar but by no means identical. It should be remembered, however, that the eigenfunction corresponding to  $\epsilon = 0.08$  is that of the inner solution, which is valid over a distance  $x = O(\epsilon^2)$  only. For any non-zero value of  $\epsilon$  there has to be a matching zone of width  $O(\epsilon)$  where the solution differs from the solution in the inner zone by a proportional difference which is  $O(1)$ . In the region where  $x/\epsilon^2$  is about 10, say,  $x/\epsilon$  is about 0.8 so that some significant differences are to be expected.

#### 4. Nonlinear stage of growth; method of calculation

To investigate the nonlinear growth of the instability we use a boundary-integral technique for numerical time stepping, essentially similar to that pioneered by Longuet-Higgins & Cokelet (1976) but in the modified form due to Vinje & Brevig (1981). The problem is formulated as finding the irrotational flow of a homogeneous, incompressible and inviscid fluid with a free surface and in infinite depth. If  $\phi(x, y, t)$  and  $\psi(x, y, t)$  denote the velocity potential and streamfunction, and  $t$  the time, then  $\phi$  and  $\psi$  are both solutions of Laplace's equation and we may write

$$\chi(z, t) = \phi + i\psi, \quad z = x + iy \quad (4.1)$$

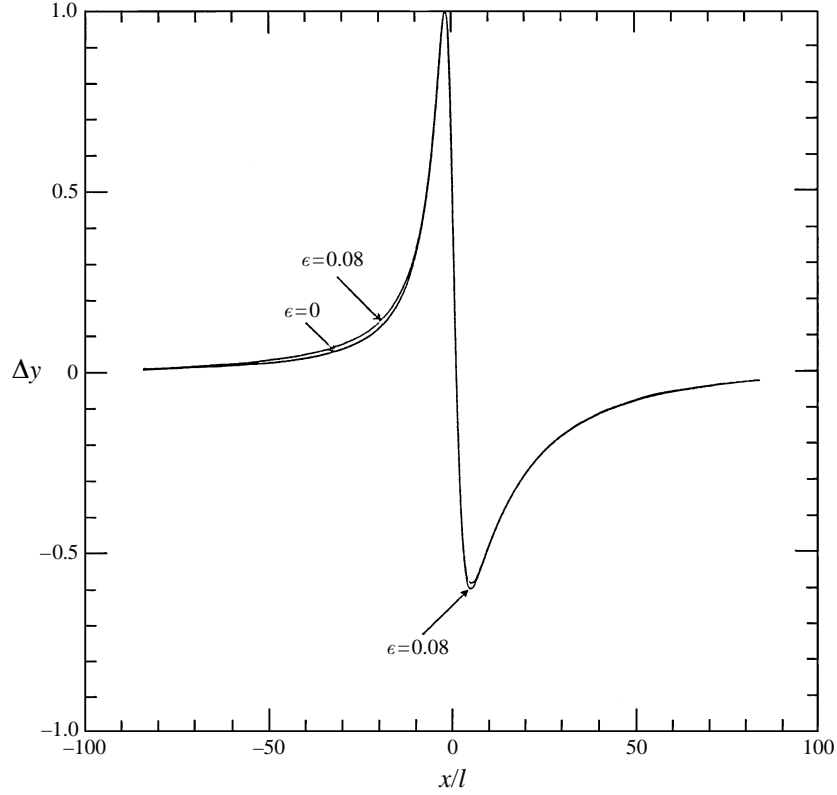


FIGURE 4. Vertical displacement  $\Delta y$  of the free surface plotted against the scaled horizontal coordinate  $x$  in the cases  $\epsilon = 0$  and  $0.08$ . The wave travels to the left.

so that  $\chi$  is an analytic function of  $z$ . At the free surface then the kinematic condition can be written

$$\frac{Dz}{Dt} = \left( \frac{d\chi}{dz} \right)^*, \quad (4.2)$$

where  $D/Dt$  denotes  $(\partial/\partial t + \nabla\phi \cdot \nabla)$  and a star denotes the complex conjugate. The condition of constant pressure can be written

$$\frac{D\phi}{Dt} = -gy + \frac{1}{2} \left| \frac{d\chi}{dz} \right|^2, \quad (4.3)$$

where  $g$  denotes gravity. We shall take  $g = 1$  and also in this application the wavelength  $L = 1$ . The mapping  $w = \exp(-2\pi iz)$  maps one wavelength onto the interior of a closed contour  $C(t)$  in the  $w$ -plane, and we may apply Cauchy's theorem

$$\chi(w, t) = \frac{1}{2\pi i} \int_C \frac{\chi(w', t)}{w' - w} dw' \quad (4.4)$$

to any point  $w$  inside  $C$ . On letting  $w$  approach  $C$  we obtain an integral equation for  $\chi$ .



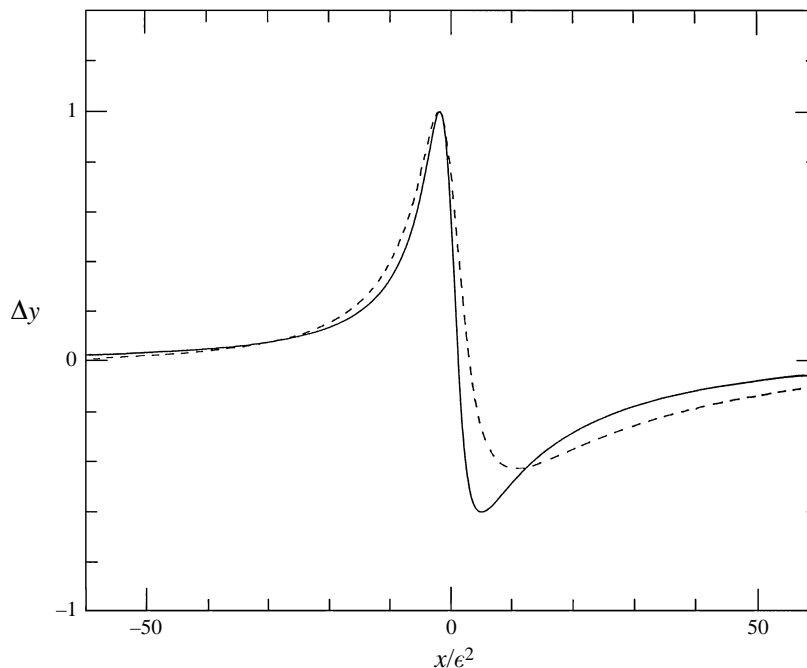


FIGURE 5. Comparison of the lowest normal-mode instability of the almost-highest wave when  $\epsilon = 0.08$  (solid curve) with the lowest instability of a periodic wave when  $\epsilon = 0.0753$  (dashed curve).

At any instant  $t$ , the boundary conditions (4.2) and (4.3) provide new values of the coordinates  $z$  and velocity potential  $\phi$  on  $C$  at the time  $(t + dt)$ . Then a discretized form of (4.4) is used to find the unknown streamfunction  $\psi$  on  $C$ . On  $C$ , piecewise-linear functions are used to represent  $\phi$  and  $\psi$ ; the resulting influence coefficients are as given in Vinje & Brevig (1981). To advance in time we use a fourth-order Runge–Kutta scheme. In order to prevent the growth of saw-tooth instabilities, five-point smoothing and re-gridding was applied after every ten time steps.

As a check on the accuracy of the method we first applied it to a steep Stokes wave with steepness parameter

$$ak = 0.43982. \quad (4.5)$$

Here  $2a$  denotes the crest-to-trough wave height and  $k = 2\pi/L$  is the wavenumber. (This corresponds to  $H/L = 0.14$ .) The wave profile was found by expanding the surface elevation and velocity potential in Fourier series with 4000 terms, and adjusting the coefficients so as to satisfy boundary conditions (for steady flow) at 4000 equally spaced grid points on the surface. To proceed with the time stepping, we used 2000 unequally spaced points; near the wave crest the spacing was reduced to provide better resolution. The smallest spacing  $\Delta x$  was  $0.61 \times 10^{-4}$  at the crest and  $0.43 \times 10^{-3}$  in the trough.

A measure of the numerical error in the Bernoulli equation is provided by the expression

$$\frac{|B + \eta + \frac{1}{2}(\nabla\phi)^2 + c\phi_x|}{|B| + |\eta| + \frac{1}{2}(\nabla\phi)^2 + c|\phi_x|} \quad (4.6)$$

which was found to be less than  $3 \times 10^{-5}$ . (Here  $B$  is the Bernoulli constant, the mean level being taken as zero.)

A further check was on the phase speed. According to the asymptotic theory of the almost-highest wave (Longuet-Higgins & Fox 1978), the speed  $c$  and steepness  $ak$  are related by equation (3.4) and

$$c^2/c_0^2 = 1.1931 - 1.18\epsilon^3 \cos(2.143 \ln \epsilon + 2.22), \quad (4.7)$$

where  $\epsilon$  is a small parameter defined by equation (2.2),  $q$  being the particle speed at the wave crest and  $c_0$  the speed of linear gravity waves ( $c_0^2 = 2\pi g/L$ ). From the initial profile we determine that  $q/c_0 = 0.12002$  and so  $\epsilon = 0.084866$ . Equations (3.4) and (4.7) then yield  $ak = 0.43966$  and  $c = 0.43589$  respectively, in good agreement with our numerically determined values; the numerically calculated speed was  $0.43589c_0$ .

## 5. Growth of normal instabilities: results

As initial condition for the normal instability at time  $t = 0$  we add to the unperturbed wave profile a perturbation  $\alpha\Delta y$  where  $\alpha$  is a small parameter and

$$\Delta y = \epsilon^2(\eta + FY_\psi)_{x=0}, \quad (5.1)$$

see (3.6) and (3.7). The velocity potential  $\phi$  in §4 is related to the potential  $\phi'$  in §§2 and 3 by  $\phi = \phi' - cx$ . Hence the perturbation in  $\phi$  is given by

$$\Delta\phi = -\epsilon^3 c\xi. \quad (5.2)$$

The two perturbations  $\Delta y$  and  $\Delta\phi$  can be given as functions of the unscaled coordinate

$$x = \epsilon^2 X \quad (5.3)$$

in the linearized approximation.

In addition, since the wavelength in §4 is taken as unity (not  $2\pi$ ),  $\Delta y$ ,  $\Delta\phi$  and  $x$  must be rescaled by multiplying by factors  $(2\pi)^{-1}$ ,  $(2\pi)^{3/2}$  and  $(2\pi)^{-1}$  respectively.

Figures 6(a) and 6(b) show the graphs of the initial perturbations  $\alpha\Delta y$  and  $\alpha\Delta\phi$  to be added to the profile and velocity potential of the steady wave, when  $\alpha = 1$ . These correspond to  $\epsilon = 0.08194$ , almost the same as in §4. The results, as we shall see, depend crucially on the sign of  $\alpha$ . Figure 7 shows the initial development of the perturbation when  $\alpha = 0.2$  (a ‘positive’ perturbation). Each curve represents the difference between the perturbed and the unperturbed surface elevation, seen in a stationary reference frame. After an initial adjustment in which the amplitude diminishes, the perturbation settles down to a steady rate of growth. This is illustrated also in figure 8, where the total range of the perturbation (i.e. the difference between the maximum and minimum elevation) is plotted versus the time  $t$  (crosses) up to  $t = 3.5$ . The dashed line shows the theoretical linear growth rate. It appears that nonlinearity affects the growth rate significantly after about  $t = 1.5$ . The initial period of adjustment may be due to the fact that the calculated eigenfunctions refer to the ‘inner’ solution of the almost-highest wave, which is valid only within a distance  $O(\epsilon^2)$  from the crest, and hence do not perfectly match the eigenfunctions for the whole wave. (The non-matching part of the initial perturbation is presumably resolved into eigenfunctions which either decay or grow less rapidly.)

The development of the complete surface profile is shown in figure 9, in the travelling reference frame. The wave clearly curls over and breaks in a characteristic way, similar to that in a solitary wave; see Tanaka *et al.* (1987, figure 5). Breaking may be said to occur when the surface profile develops a sharp corner at around  $t = 2.0$ .

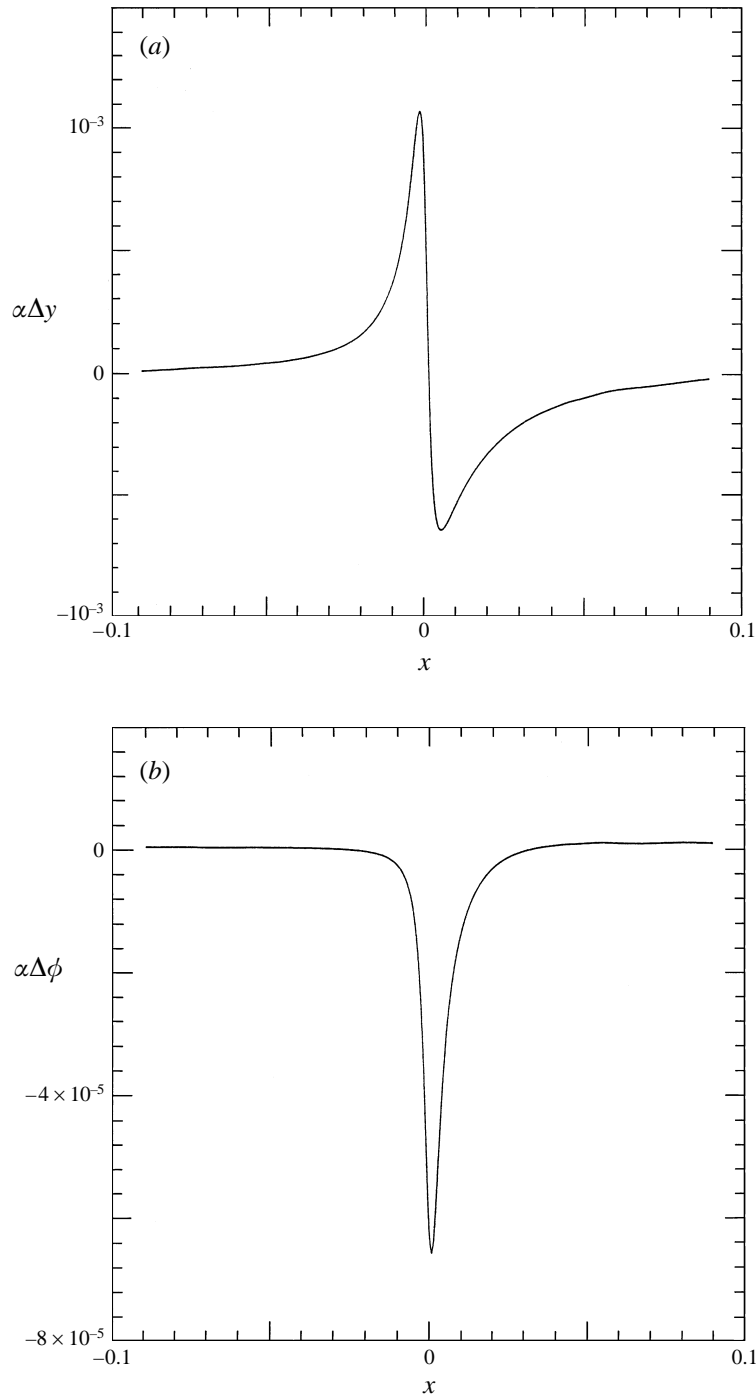


FIGURE 6. Form of the initial perturbations when  $\alpha = 1$ , as functions of the unscaled horizontal coordinate  $x$ : (a)  $\Delta y$ , (b)  $\Delta\phi$ .

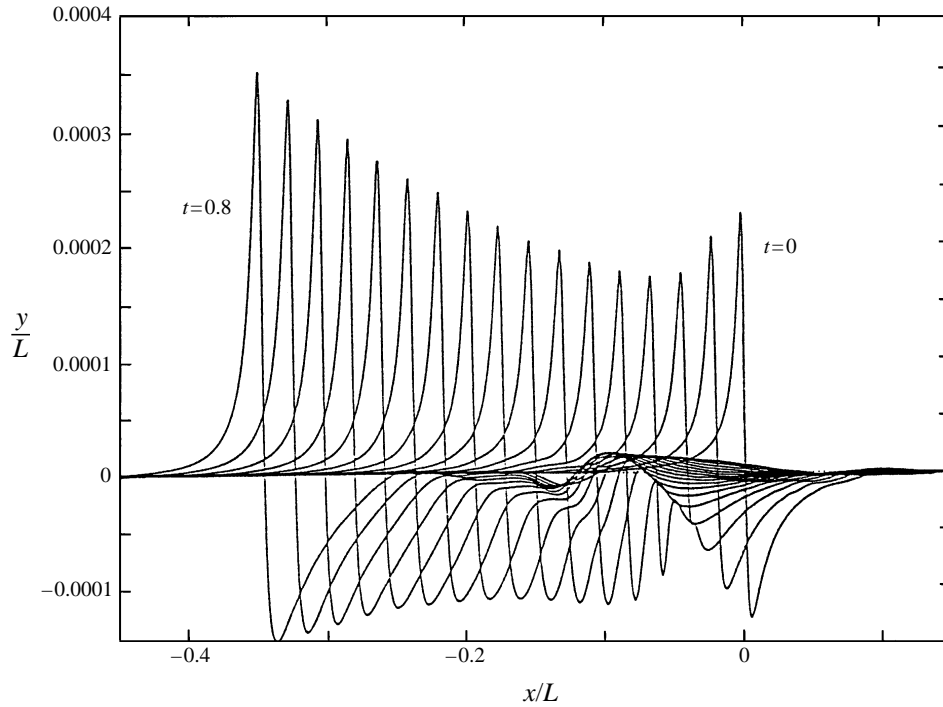


FIGURE 7. Initial development of the positive perturbation, when  $\alpha = 0.2$ , in a moving reference frame.

The development of the *negative* perturbation corresponding to  $\alpha = -0.2$  is more interesting and is shown first in figure 10. After a similar initial period of adjustment the perturbation grows exponentially, as expected; see the plotted points (squares) in figure 8. The departures from the linear growth rate are of similar magnitude, but opposite sign, to the positive perturbation.

With the negative perturbation, however, the surface profile remains convex and rounded, as seen in figure 11. By analogy with the solitary wave (Tanaka *et al.* 1987) we would expect the initial perturbed curve to undergo a transition to a lower wave of the same total energy  $E$  as the original. From the asymptotic formulae for the potential and kinetic energies given in Longuet-Higgins & Fox (1978) we find for the total energy density ( $T+V$ )

$$E = 0.07286 - 0.383 \epsilon^3 \cos(2.143 \ln \epsilon + 1.59). \quad (5.4)$$

Figure 12 shows  $E$  as a function of the wave steepness  $ak$ . Thus the initial wave, for which  $ak = 0.4398$  and  $\epsilon = 0.08487$ , has an energy  $E = 0.07306$ , which is the same as that of a lower wave with  $\epsilon = 0.2239$  and hence  $ak = 0.4182$  ( $H/L = 0.1331$ ).

The actual long-term development of the negative instability is shown in figures 13 and 14. Figure 13 shows the crest-to-trough wave height  $2a$  as a function of the time, and figure 14 shows the phase difference, as measured by the position of the maximum elevation of the crest. From figure 13 it appears there is indeed a transition to a lower wave of height 0.1303, approximately as expected, but that the wave then returns almost to the original height, in a kind of recurrence, and then oscillates. The difference in phase speed relative to the original wave may be measured by the gradient of the

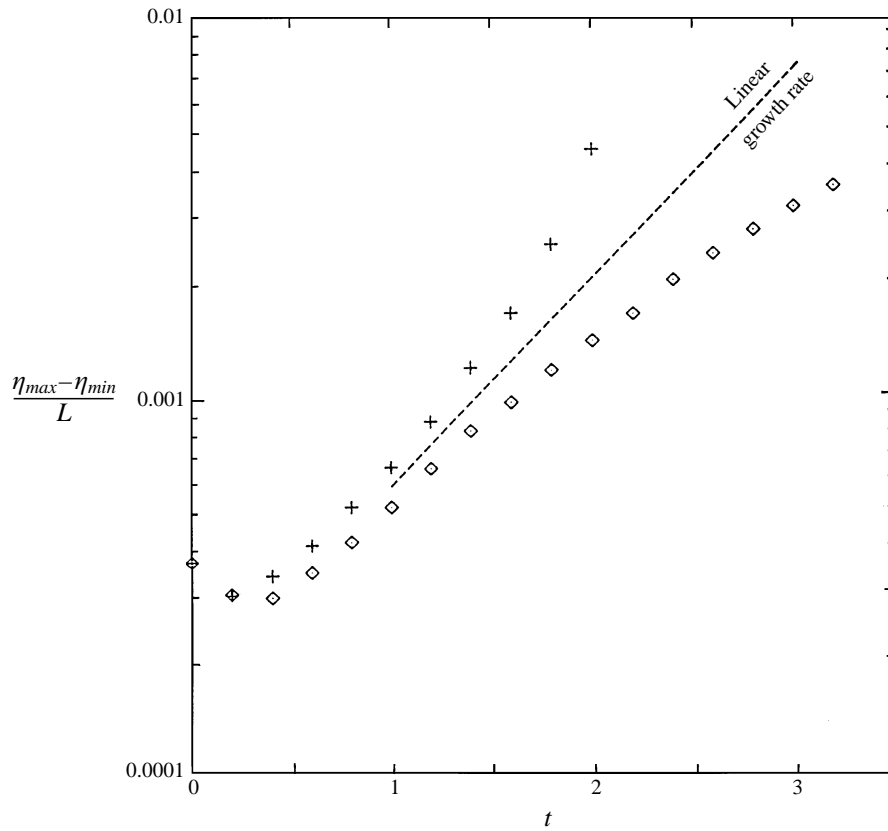


FIGURE 8. Range of the perturbations as a function of the time  $t$ . Positive and negative perturbations ( $\alpha = \pm 0.2$ ) are marked by crosses and square plots, respectively.

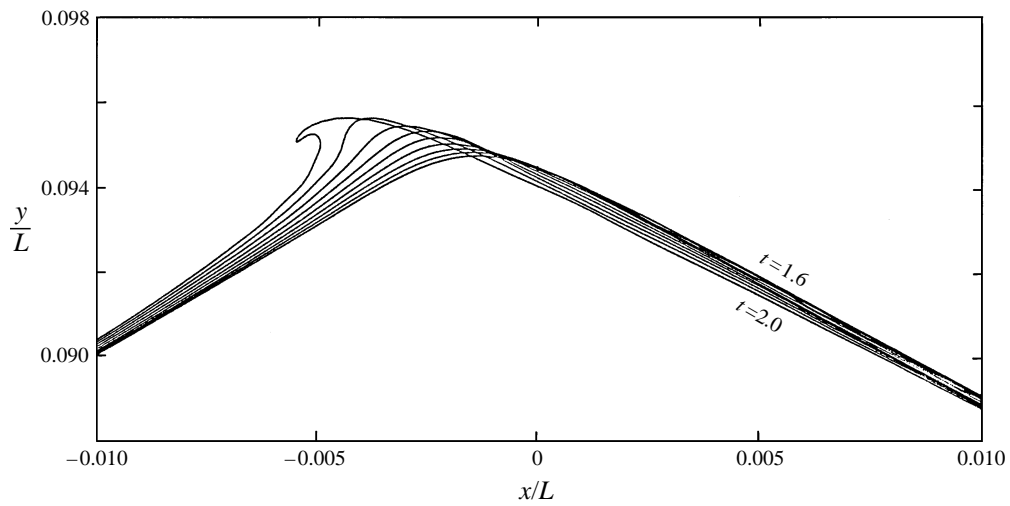


FIGURE 9. Development of the surface profile after the positive perturbation ( $\alpha = 0.2$ ) at time intervals  $\Delta t = 0.05$ , as seen in a reference frame moving with the phase speed of the unperturbed wave.

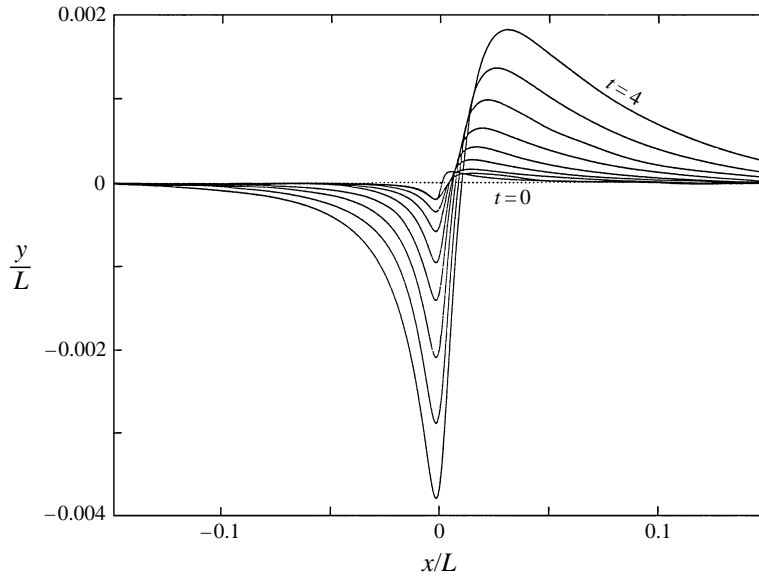


FIGURE 10. Development of the negative perturbation, when  $\alpha = -0.2$ , in the moving reference frame of figure 9.

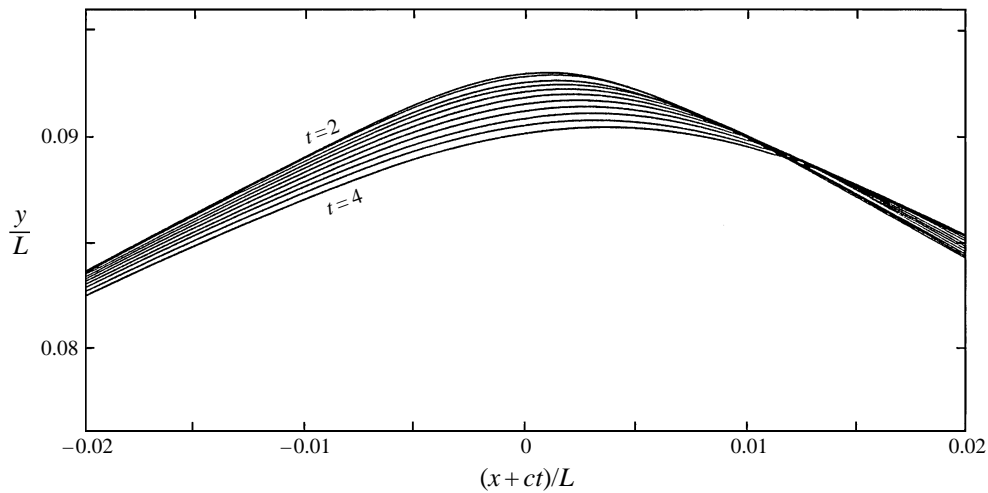


FIGURE 11. Development of the surface profile after the negative perturbation ( $\alpha = -0.2$ ) at time intervals  $\Delta t = 0.2$ , as seen in the moving reference frame.

curve in figure 14. The *maximum* gradient corresponds to a difference  $\Delta c = 0.0016$  hence  $(2\pi)^{1/2}\Delta c = -0.0040$  and this does agree roughly with the difference in speeds

$$\Delta c = c_1 - c_2 = -0.0037, \quad (5.5)$$

see table 3. However, in figure 14 the maximum phase-speed difference is at around  $t = 5$ , which is not when the wave has its minimum amplitude. Also there is an interval of time near  $t = 8$  where  $\Delta c$  is apparently negative. Thus the phenomenon is less simple than it appears at first.

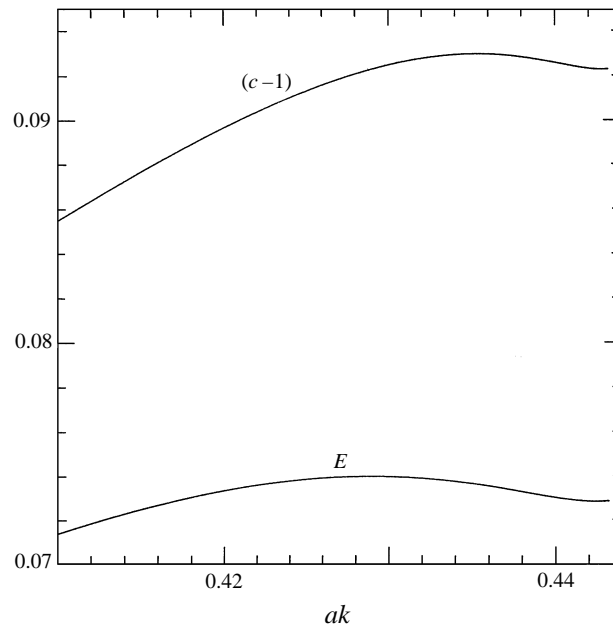


FIGURE 12. The total energy  $E$  and the phase speed  $c$  as functions of the wave steepness  $ak$ .

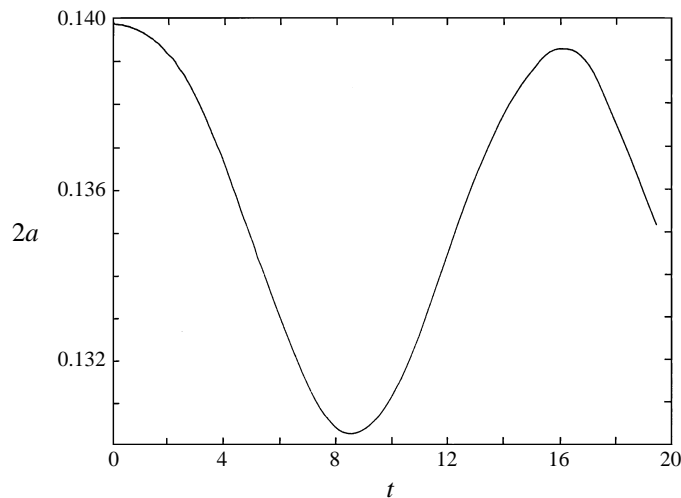
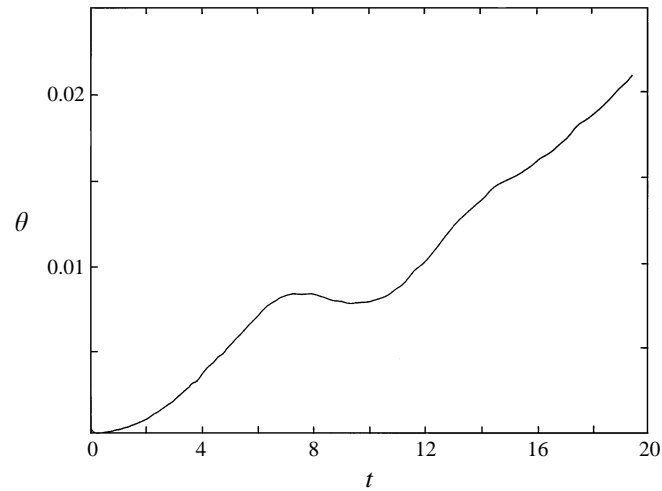
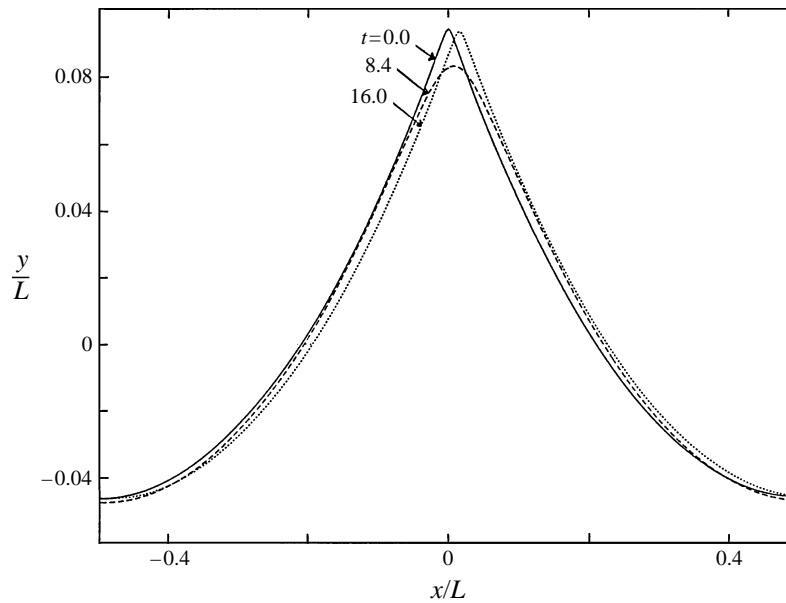


FIGURE 13. Crest-to-trough height of the perturbed wave, as a function of the time  $t$ .

Figure 15 shows the complete surface profiles at times  $t = 0, 8.4$  and  $16.0$ , the vertical scale being exaggerated. The recurrent character of the transition is clearly different from the corresponding behaviour in the case of the solitary wave (Tanaka *et al.* 1987) where the wave height tends to its lower value exponentially in time. As a check on the accuracy of the numerical time stepping in figures 13 and 14, we note that the total energy at time  $t = 19.6$  was  $1.85022 \times 10^{-3}$  compared with the initial energy  $1.85031 \times 10^{-3}$  at time  $t = 0$ , a proportional difference of less than  $5 \times 10^{-5}$ .

FIGURE 14. Phase of the perturbed wave, as a function of the time  $t$ .FIGURE 15. Surface profiles at times  $t = 0, 8.4$  and  $16.0$ . The vertical scale is enlarged.

---

$\epsilon$	$ak$	$H/L$	$E$	$c/c_0$
0.08487	0.43982	0.1400	0.07306	1.09262
0.22400	0.41818	0.1331	0.07306	1.08894

---

TABLE 3. Comparison of wave parameters

## 6. Discussion and conclusions

Previous calculations of the normal-mode instabilities of the ‘almost-highest wave’ have been revised. The rate of growth of the fastest-growing mode agrees well with recent calculations by Tanaka (1995) (see Longuet-Higgins & Tanaka 1997) and



provides an asymptote for them as the crest parameter  $\epsilon = q\sqrt{2c_0}$  tends to zero. The limiting form of the lowest normal-mode instability is as close as can be expected to that computed by Tanaka for  $\epsilon = 0.0753$  (the smallest value of  $\epsilon$  for which he made calculations).

Time stepping of the initially perturbed wave by a boundary-integral method has shown that the subsequent development of the instability at first follows the linear theory faithfully. The subsequent nonlinear stages of growth depend crucially on the sign of the initial perturbation. ‘Positive’ perturbations lead to overturning of the wave crest; ‘negative’ perturbations lead on to a transition of the wave to an almost steady wave of lower amplitude, followed by a kind of recurrence, the wave returning very nearly to its initial height and speed.

This behaviour differs from that found for the solitary wave by Tanaka *et al.* (1987), where a negative perturbation led to a monotonic transition to a lower solitary wave. It might be considered that in that case the period of recurrence was infinitely long.

Our results also differ from those of Jillians (1989) who did not report recurrence, possibly owing to his use of a larger initial perturbation.

Finally it must be emphasized that the type of motion considered in the present paper is purely irrotational flow without surface tension or viscosity. Especially in the case of the positive perturbation, surface tension can be expected to have important effects on the ‘jet’ of the overturning breaker, particularly when the wavelength  $L$  is less than about 2 m, and may prevent it from plunging altogether; see Duncan *et al.* (1994). At a later stage in the process, vorticity can be introduced by viscous dissipation, leading to a capillary roller (Longuet-Higgins 1992). These effects are at present under investigation.

By arrangement with Professor Peregrine, M. Jervis has applied the perturbations shown in our figure 6 to steep solitary waves, obtaining results similar to those described by Tanaka *et al.* (1987). M.S.L.-H. is supported by the Office of Naval Research under Contract N00014-91-J-1582 and D.G.D. under Contract N00014-93-C-0046.

#### REFERENCES

- CLEAVER, R. P. 1981 Instabilities of gravity waves. PhD thesis, University of Cambridge.
- DUNCAN, J. H., PHILOMIN, V., QIAO, H. & KIMMEL, J. 1994 The formation of a spilling breaker. *Phys. Fluids* **6**, S2.
- JILLIANS, W. J. 1989 The superharmonic instability of Stokes waves in deep water. *J. Fluid Mech.* **204**, 563–579.
- LONGUET-HIGGINS, M. S. 1992 Capillary rollers and bores. *J. Fluid Mech.* **240**, 659–679.
- LONGUET-HIGGINS, M. S. & CLEAVER, R. P. 1994 Crest instabilities of gravity waves. Part 1. The almost-highest wave. *J. Fluid Mech.* **158**, 115–129.
- LONGUET-HIGGINS, M. S., CLEAVER, R. P. & FOX, M. J. H. 1994 Crest instabilities of gravity waves. Part 2. Matching and asymptotic analysis. *J. Fluid Mech.* **259**, 333–344.
- LONGUET-HIGGINS, M. S. & COKELET, E. D. 1976 The deformation of steep surface waves on water. I. A numerical method of computation. *Proc. R. Soc. Lond. A* **350**, 1–26.
- LONGUET-HIGGINS, M. S. & FOX, M. J. H. 1977 Theory of the almost-highest wave: the inner solution. *J. Fluid Mech.* **80**, 721–741.
- LONGUET-HIGGINS, M. S. & FOX, M. J. H. 1978 Theory of the almost-highest wave. Part 2. Matching and analytic extension. *J. Fluid Mech.* **259**, 333–344.
- LONGUET-HIGGINS, M. S. & TANAKA, M. 1997 On the crest instabilities of steep surface waves. *J. Fluid Mech.* **336**, 51–68.

- SAFFMAN, P. G. 1985 The superharmonic instability of finite-amplitude water waves. *J. Fluid Mech.* **159**, 169–174.
- TANAKA, M. 1983 The stability of steep gravity waves. *J. Phys. Soc. Japan* **52**, 3047–3055.
- TANAKA, M. 1986 The stability of solitary waves. *Phys. Fluids* **29**, 650–655.
- TANAKA, M. 1995 On the “crest instabilities” of steep gravity waves. *Proc. Workshop on Mathematical Problems in the Theory of Nonlinear Water Waves, CIRC, Luminy, France, 15–19 May 1995*.
- TANAKA, M., DOLD, J. W., LEWY, M. & PEREGRINE, D. H. 1987 Instability and breaking of a solitary wave. *J. Fluid Mech.* **185**, 235–248.
- VINJE, T. & BREVIG, P. 1981 Breaking waves on finite water depths: a numerical study. *Ship Res. Inst. of Norway, Rep. R-111.81*.